Check for updates

The relationship between bone, hemopoietic stem cells, and vasculature

Sarah L. Ellis,[1-3] Jochen Grassinger,[4] Allan Jones,[5] Judy Borg,[1] Todd Camenisch,[6] David Haylock,[7] Ivan Bertoncello,[3] and Susan K. Nilsson[3,7]

[1]Peter MacCallum Cancer Centre, Melbourne, Australia; [2]Australian Stem Cell Centre, Clayton, Australia; [3]University of Melbourne, Parkville, Australia; [4]University of Regensburg Medical Centre, Regensburg, Germany; [5]University of Sydney, Sydney, Australia; [6]College of Pharmacy, University of Arizona, Tucson, AZ; and [7]Commonwealth Scientific and Industrial Research Organisation, Clayton, Australia

A large body of evidence suggests hemopoietic stem cells (HSCs) exist in an endosteal niche close to bone, whereas others suggest that the HSC niche is intimately associated with vasculature. In this study, we show that transplanted hemopoietic stem and progenitor cells (HSPCs) home preferentially to the trabecular-rich metaphysis of the femurs in nonablated mice at all time points from 15 minutes to 15 hours after transplantation. Within this region, they exist in an endosteal niche in close association with blood vessels. The preferential homing of HSPCs to the metaphysis occurs rapidly after transplantation, suggesting that blood vessels within this region may express a unique repertoire of endothelial adhesive molecules. One candidate is hyaluronan (HA), which is highly expressed on the blood vessel endothelium in the metaphysis. Analysis of the early stages of homing and the spatial distribution of transplanted HSPCs at the single-cell level in mice devoid of Has3-synthesized HA, provides evidence for a previously undescribed role for HA expressed on endothelial cells in directing the homing of HSPCs to the metaphysis. (*Blood*. 2011;118(6):1516-1524)

Introduction

Hemopoietic stem cells (HSCs) exist in a specialized microanatomic space within the bone marrow (BM) termed the niche.[1] Within the niche, cues from the surrounding microenvironment maintain the balance between maintenance of the stem cell pool and proliferation. Despite 30 years of research, the precise location of the HSC niche is unclear. Using different phenotypic markers for hemopoietic stem and progenitor cells (HSPCs), many groups have attempted to define the location of the HSC niche based on its cellular constituents. As examples, the endosteal or osteoblastic niche suggests that HSCs are close to or touching osteoblasts,[2-5] and the vascular niche suggests that HSCs are close to or in contact with the sinusoidal endothelium.[6,7] Considerable debate has ensued regarding the prominence of each of these niches in HSC regulation. However, several critical questions remain unanswered, including the following: Are these separate or overlapping niches? Do HSCs actually have to be in contact with particular cell types for HSC regulation? Is one cell type more important than others in regulating HSC? Of paramount importance to addressing these questions is an understanding of the three-dimensional relationship between HSCs, blood vessel (BVs), and bone.

Most recently, intravital 2-photon or confocal microscopy was used to define the HSC niche by investigating the spatial distribution and lodgement of transplanted fluorescently labeled HSPCs.[7-10] However, the thick cortical bone of long bones presents a challenge for current high resolution imaging modalities as it is impervious to light. A number of innovative methodologies have recently been developed by researchers to permit imaging of HSPC homing to their niche in long bones either in vivo[8,11] or ex vivo.[10,12] These consist of cutting or splitting the bone,[10,12] grinding the cortical bone until semitransparent,[8] or inserting an imaging probe into the BM.[11] As the vasculature of the bone is continuous with the BM,[13] damaging bone disrupts BM vasculature, inducing a stress response. Stress responses include the up-regulation of the chemokine, stromal derived factor 1 (SDF-1),[14,15] and vascular cell adhesion molecule 1 (VCAM-1),[11,16] both of which are important to HSPC homing and may affect the spatial distribution of transplanted HSPCs. In addition, intravital imaging cannot visualize HSPCs deep within BM of long bones and only visualizes small areas. These limitations prevent HSPC homing investigation throughout the entire length and depth of cellular marrow in long bones and subsequent resolution of the topologic relationship between HSPCs and their niche in 3 dimensions.

To overcome the problems associated with imaging long bones, others have investigated the homing of HSPCs in calvarium of nonablated recipients, which is largely trabecular bone and thin enough to permit optical imaging with minimal manipulation.[7,9,17] Using this model, transplanted HSPCs were demonstrated to reside within 50 μm, but not < 30 μm, of bone in a combined vascular and endosteal niche.[9] However, it is unclear whether these results can be extended to long bones where 86.5% of cellular marrow is considered central marrow.[18]

We have developed a unique approach to investigate the microanatomic location of HSPCs with respect to BV and bone in long bones without damage to either the bone or BM. We use a combination of micro-computed tomography (CT), histomorphometry, homing, and spatial distribution assays to provide detailed analysis of the location of individual HSPCs at short time points after transplantation in physiologic conditions. We show that high proportions of HSPCs home preferentially to the trabecular-rich metaphysis of long bones at all time points examined, 15 minutes to

Submitted August 25, 2010; accepted May 26, 2011. Prepublished online as *Blood* First Edition paper, June 14, 2011; DOI 10.1182/blood-2010-08-303800.

The online version of this article contains a data supplement.

The publication costs of this article were defrayed in part by page charge payment. Therefore, and solely to indicate this fact, this article is hereby marked "advertisement" in accordance with 18 USC section 1734.

© 2011 by The American Society of Hematology

Downloaded from http://ashpublications.net/blood/article-pdf/118/6/1516/1347016/zh803211001516.pdf by guest on 02 June 2024

15 hours after transplantation. We reveal that HSPCs within the metaphysis reside in an endosteal niche in close association with BVs. We also illustrate that, although BVs within this region are integral to the HSPC niche, they do not form a separate niche. To determine the mechanism underpinning the preferential homing of HSPCs to trabecular bone, we examine adhesion molecules on the sinusoidal endothelium for differential expression, as has previously been observed in the calvarium.[7] We demonstrate that hyaluronan (HA) produced by Has3 synthase is important for HSPC transendothelial migration within the metaphysis during early stages after transplantation. Consistent with studies conducted on calvarium,[7] these data suggest that BM BVs are specialized with regards to their expression of adhesion molecules and are important in HSPC homing to their endosteal niche.

Methods

Mice

Mice were either bred at or purchased from Monash Animal Services (Monash University, Victoria, Australia). $Opn^{-/-}$ mutant mice were provided by Dave Denhardt (Rutgers University) and $Has3^{-/-}$ mutant mice by Todd Camenisch (College of Pharmacy, Tucson, AZ). All strains are maintained on a C57BL/6 background, and all experiments were approved by the Monash Animal Services Ethics Committee.

Isolation of enriched populations of HSPCs

Populations of HSPC ($Lin^-Sca^+Kit^+$ [LSK]) were isolated by flow cytometric cell sorting as previously described.[19] Briefly, low density Lin^- BM cells were labeled with a cocktail of Sca-1–PacificBlue (BioLegend) and c-kit–allophycocyanin (BD Biosciences PharMingen).

Flow cytometry

HSPCs were sorted and reanalyzed for purity on a Cytopeia Influx 516SH cell sorter (Cytopeia). Pacific Blue conjugates were excited with the 405-nm laser and fluorescence emission detected with 460 ± 25-nm band pass filter. Allophycocyanin conjugates were excited with the 635-nm laser and fluorescence emission detected with 660 ± 10-nm band pass filter.

Flow cytometric analysis after transplantation was performed using a BD LSR II analyser (BD Biosciences) using a 488-nm laser in conjunction with a 528 ± 38-nm band pass filter.

Labeling of HSPCs with carboxyfluorescein diacetate-succinimidyl ester

HSPCs were labeled with the fluorescent tracking dye CFSE (Invitrogen) at a final concentration of 0.5μM as previously described.[20]

Homing and spatial distribution assays

$CFSE^+$ HSPCs ($4\text{-}18 \times 10^4$) were cotransplanted into nonirradiated recipients via lateral tail vein injection with 200 000 unlabeled BM filler cells in 200 μL phosphate-buffered saline per recipient. The homing efficiency and spatial distribution of transplanted HSPCs at various time points after transplantation were assessed as previously described.[20] Briefly, one leg was removed and BM harvested to assess HSPC homing. For this, the proportion of transplanted cells homed to BM was calculated using the total white blood cell count as the denominator and assuming that cells from one femur, tibia, and iliac crest represent approximately 15% of total BM.[21] The second leg was perfused via the descending dorsal aorta with 4% weight/volume paraformaldehyde at physiologic pressure before excising the femur, decalcifying in 10% EDTA (Sigma-Aldrich) and processing for routine histology. Care was taken to ensure that complete longitudinal sections through the middle of the femur were obtained for spatial distribution analyses. Alternate sections were examined to prevent recording the same transplanted HSPCs twice.

Preparation of femoral BVs for histomorphometry.

Mice were injected intraperitoneally with 500 IU of heparin (Pharmacia) 30 minutes before perfusion. After anesthesia, perfusion of warm fixative consisting of paraformaldehyde (2% volume/volume) and glutaraldehyde (2.5% volume/volume) was performed as described in "Homing and spatial distribution assays." After fixation, femurs were removed, decalcified as described in "Homing and spatial distribution assays," postfixed in 2% osmium tetroxide, and embedded in Spurr resin. Transverse or longitudinal 1-μm sections were stained with 1% sodium tetraborate, 1% Azur II, 1% toluidine blue in distilled water. Ultrathin sections were cut using an Ultracut S ultramicrotome (Leica), contrasted with uranyl acetate and lead citrate and examined in a JEOL 1011 transmission electron microscope.

Microvascular casting

Mice were heparinized and perfusion-fixed as described in "Homing and spatial distribution assays," before perfusing with Mercox (CL-2B blue color; Ladd Research) in the presence of the catalyst, benzoyl peroxide (0.5 g/20 mL Mercox). Mice were left at room temperature for 1 hour before the hind legs were removed and placed in fresh fixative overnight. Femurs were dissected, decalcified as described in "Homing and spatial distribution assays," and placed in 20% KOH at 45°C for 2 weeks until all tissue was dissolved. Vascular casts were air dried and examined in a NeoScope (JEOL/Nikon Instruments) scanning electron microscope with an accelerating voltage of 10 kV.

Immunohistochemistry

Immunolabeling of longitudinal femoral sections was performed as previously described[19] with the exception that antigen retrieval was by heating sections in 10mM citrate buffer (pH 6.0). Sections were incubated with antibodies to adhesion molecules or isotype controls followed by biotinylated secondary antibodies (supplemental Table 1, available on the *Blood* Web site; see the Supplemental Materials link at the top of the online article). Signal was amplified using tyramide signal amplification or tyramide signal amplification plus Cyanine 3 (TSA Plus; PerkinElmer Life and Analytical Sciences) according to the manufacturer's instructions. Biotinyl-tyramide was visualized using steptavidin-Alexa488 or steptavidin-Alexa568 at a dilution of 10 μg/mL (Invitrogen). Sections were mounted in Vectashield Hard Set mounting medium with 4,6-diamidino-2-phenylindole (Vector Laboratories). Antibody to ICAM-2, or its isotype control, was injected into the tail vein of mice at a dose of 1 to 2 mg/kg. After 15 minutes, mice were perfused with fixative, paraffin-embedded, and sections labeled with the appropriate secondary antibodies followed by signal amplification as detailed earlier in this paragraph. Staining for HA and osteopontin (Opn) was as detailed earlier in this paragraph with the exception that biotinylated secondary antibody was not required for HA.

Recording of images

Immunofluorescent images were recorded using a SPOT RT-SE6 Slider cooled CCD camera (Diagnostic Instruments) fitted on an Olympus BX51 microscope equipped with conventional epifluorescence. Montages of resin sections were recorded with an Orca-ER-cooled CCD camera fitted on an Olympus IX81 microscope . Electron micrographs were recorded with a MegaView III CCD cooled digital camera (Soft Imaging Systems).

Micro-CT

Perfusion-fixed femurs were scanned with a Skyscan 1172 high-resolution Micro-CT system (Skyscan) using a 5-μm focal spot size. X-rays were produced by exposing the anode to 59 kV at 167 μA, and bones were scanned at 0.2° rotation steps over 360° rotation. Images were converted to axial slices (N-Recon; Skyscan) for subsequent bone morphometric analysis of trabeculae separation (CTAn; Skyscan). Three-dimensional reconstructions were achieved using Imaris Version 6.1.5 software (Bitplane).

Downloaded from http://ashpublications.net/blood/article-pdf/118/6/1516/1347016/zh803211001516.pdf by guest on 02 June 2024

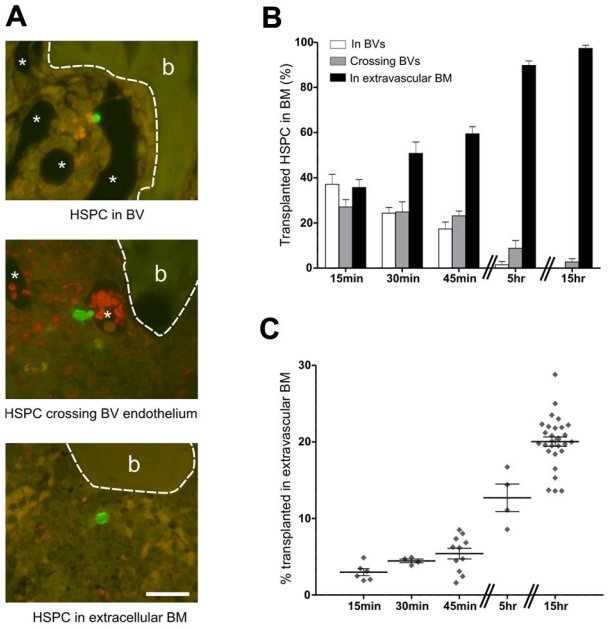

Figure 1. Transplanted HSPCs home rapidly to the BM where analysis of the spatial distribution of individual HSPCs reveals their location and allows an accurate assessment of homing efficiency. (A) At 15 minutes after transplantation, HSPCs are already in the BM and are classified as being within BVs (top image), crossing BV endothelium (middle image), or being within the extravascular space (bottom image). Because of perfusing the fixative through the BVs, these structures are mostly cleared of blood. The thin-walled endothelium is visible at higher magnification (not shown). In the middle micrograph, red blood cells remaining in the BV are distinguished by their reddish hue, which is a result of the dual filter used to visualize the images. *BV. Bone (b) is outlined by a dashed line. Scale bar represents 25 μm. Micrographs captured using a 60× (UPlanApo NA 1.2) objective on an Olympus BX51 microscope fitted with a SPOT RT-SE6 camera. (B) The percentage of HSPCs in each of these areas during the first 15 hours after transplantation is shown: 15 minutes, n = 7 (424 HSPCs); 30 minutes, n = 6 (287 HSPCs); 45 minutes, n = 8 (605 HSPCs); 5 hours, n = 3 (129 HSPCs); and 15 hours, n = 5 (635 HSPCs). (C) Homing efficiencies determined by flow cytometry were corrected for the percentage of HSPCs in vessels. Symbols represent individual recipients. (B-C) Experimental repeats are ≥ 2. Data are mean ± SEM.

Histomorphometry

Distances between BVs in the metaphysis were calculated using Metamorph (Molecular Devices) as detailed in supplemental Table 2. The average width of individual BVs, numbers of BVs per millimeter squared, and proportion of marrow in the metaphysis compared with the diaphysis were calculated using Metamorph.

Statistical analysis

Data are presented as mean ± SEM. Differences between means were evaluated by either a Student unpaired *t* test or a 1-way ANOVA and considered statistically significant at a *P* value of $< .05$. Statistical analyses were performed with Prism Version 5 (GraphPad).

Results

Transplanted HSPCs rapidly home to BM and can be visualized as they transendothelially migrate

At 15 minutes after transplantation, HSPCs were observed within BM vasculature (Figure 1A top), crossing the sinusoidal endothelium (Figure 1A middle) and within BM extravascular space (Figure 1A bottom). Recording the precise location of individual transplanted HSPCs as within BVs, crossing BV endothelium or within BM is unique to this study and provides an accurate snapshot of the early stages of HSPC homing. BVs were identified at high magnification by the presence of endothelial cells. The spatial distribution of 2080 transplanted HSPC was recorded at the single-cell level over the first 15 hours after transplantation. A minimum of 6 alternate sections through the middle of the femur were examined with at least 35 transplanted HSPCs counted per recipient. HSPCs observed within perfused sinusoids were in contact with endothelial cells, suggestive of an adhesive interaction. Over time, the numbers of HSPC in sinusoids and crossing the sinusoidal endothelium decreased until, by 15 hours, these were rarely observed (Figure 1B). HSPCs were observed as single cells, with only 2 instances of HSPC pairs observed, both in the extravascular marrow 15 hours after transplantation. The mean diameter of HSPCs in sections is 5.5 ± 0.14 μm (n = 34) with HSPCs in the process of diapedesis elongating and reaching more than twice this size in length.

Recording the proportions of HSPCs within BVs at each time point and taking this figure into account for analyses of flow cytometric-derived homing data enabled a more precise measurement of HSPC homing to BM from 15 minutes (3% ± 0.4%) to 15 hours (20% ± 0.6%; Figure 1C).

Transplanted HSPCs preferentially home to the trabecular-rich metaphysis

The femur is divided into 3 anatomic regions: the epiphyses, metaphyses, and diaphysis (Figure 2A). The epiphyses lie on either side of the growth plates at the extremities of the femur, the trabecular-rich metaphyses form the growing portion of the bone, and the diaphysis is the main central bone shaft.[13] Analysis of the

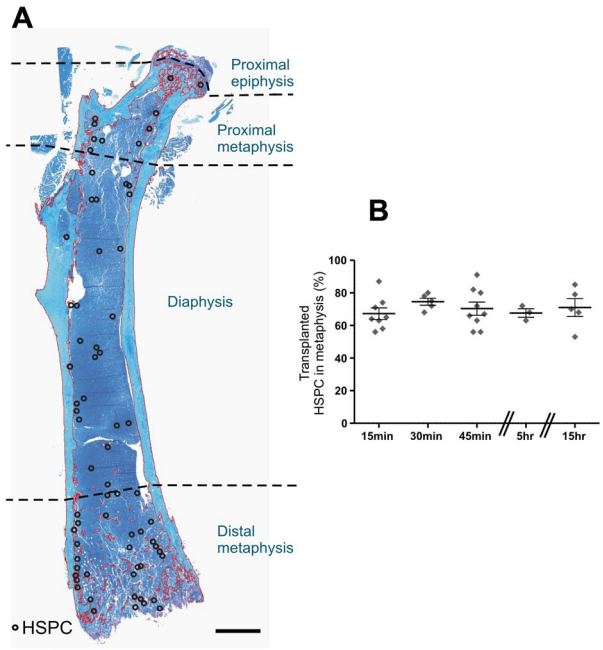

Figure 2. Transplanted HSPCs home preferentially to the trabecular-rich metaphysis. (A) Spatial distribution map of individual HSPCs within the femur 15 hours after transplantation. The map was constructed by transposing the spatial distribution of individual HSPCs (○) from 5 alternate serial sections onto a representative section taken from the beginning of the series. Toluidine blue stain. Scale bar represents 1 mm. Micrograph captured using a 10× (UPLSApo NA 0.4) objective on an Olympus BX51 microscope fitted with a SPOT RT-SE6 camera. Montage constructed with Photoshop CS2. (B) The spatial distribution of individual HSPCs from longitudinal sections of femur demonstrates a preferential distribution of HSPCs to the trabecular-rich metaphysis. Each symbol represents an individual recipient. Experimental repeats more than or equal to 2. Data are mean ± SEM.

Downloaded from http://ashpublications.net/blood/article-pdf/118/6/1516/1347016/zh803211001516.pdf by guest on 02 June 2024

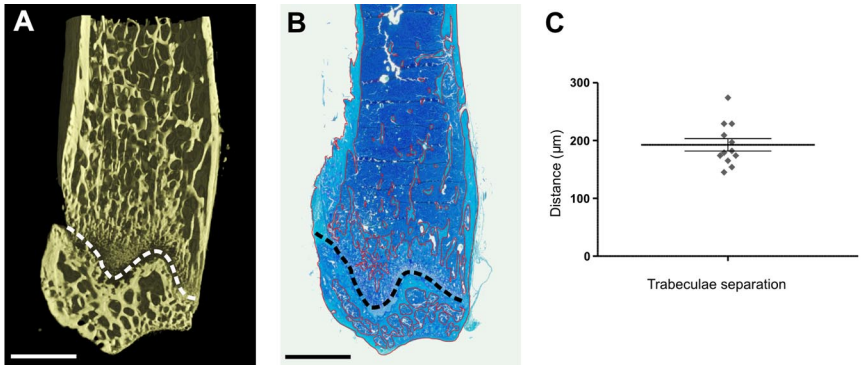

Figure 3. HSPCs within the metaphysis exist in an endosteal niche. (A) Micro-CT image of the distal region of a murine femur, revealing the dense interconnecting network of trabeculae. (B) Montage of a toluidine blue-stained paraffin wax section of the distal metaphysis of the exact same murine femur as in the adjacent micro-CT image after histologic processing. The trabeculae are delineated in red using Metamorph software and appear more sparsely distributed than in the more detailed 3D micro-CT image. (A-B) The growth plate is delineated by the dashed line. Above the growth plate is the metaphysis, and below the growth plate is the epiphysis. Scale bar represents 1 mm. (C) Analysis of micro-CT 3D images reveals the distance separating trabeculae. The 12 data points represent individual measurements from the proximal and distal metaphysis from 6 mice. Data are mean ± SEM.

precise location of 2426 individual HSPCs from 30 recipients revealed transplanted HSPCs preferentially home to the trabecular-rich metaphyses at all time points examined with an average of 71% ± 1.8% homing to this region within 15 hours (Figure 2B).

HSPCs within the metaphysis exist in an endosteal niche and are close to blood vessels

Traditionally, the spatial distribution of transplanted HSPCs has been classified as being either central or endosteal based on a variety of definitions of "endosteal." In our and other laboratories,[22-24] the endosteal region is arbitrarily defined as within 12 cell diameters (~ 96 μm) of bone.[3] Classifying transplanted HSPCs within trabecular-rich regions of bone as either central or endosteal cannot take into account trabecular bone lying just outside the plane of section. In contrast, micro-CT reveals in 3D the dense interconnecting network formed by trabeculae within the metaphysis providing greater precision than routine histology (Figure 3A and B, respectively). With micro-CT, the distance separating individual trabeculae within the metaphysis was determined to be 192 ± 10.7 μm demonstrating that mathematically all cells within the metaphysis are within 96 μm or < 12 cell diameters from bone (average cell diameter ~ 8 μm) and reside in an endosteal niche (Figure 3C).

To discern the microanatomic relationship between BM vasculature and bone, we performed histomorphometry on femoral resin sections. The preservation of BVs within resin sections was evaluated with transmission electron microscope before performing histomorphometric analyses. Embedding bones in resin minimized compression during sectioning and ensured vessels did not collapse (Figure 4A). Using light microscopy, endothelial cells lining BVs were clearly visible at high magnification without the need for endothelial cell staining. Osmium postfixation preserved the lipids and rendered them distinct from BVs (Figure 4E) because they appear opaque. Metaphyseal vessels run predominately parallel to the long axis of cortical bone, whereas diaphyseal sinusoids are arranged centrifugally around the central sinus perpendicular to the long axis of cortical bone.[13,25] The different arrangement of vessels between the metaphysis and diaphysis was an important consideration when measuring BV parameters. To ensure that measurements were made primarily on sinusoids in cross-sectional profiles, transverse sections were cut of the metaphysis and longitudinal sections were cut of the diaphysis (Figure 4B and C, respectively). The size of BVs varied within transverse sections of the metaphysis (Figure 4D-E) with larger vessels more frequently observed further from the growth plate because of branching of the main central sinus as it ramifies throughout the metaphysis. Smaller vessels were predominant adjacent to cortical bone in this area. To ensure that representative measurements of BVs within the metaphysis, histomorphometric analyses were performed on at least 2 femoral sections from each mouse at varying distances from the growth plate. Measurements of the distance separating BVs assumes they are predominantly round and evenly distributed (Figure 4D-E). The distance separating BVs within the metaphysis is 45 ± 2 μm (n = 10), revealing that all cells in the metaphysis are within 18.5 μm or < 3 cells of a BV (Figure 4F). Scanning electron microscopy of vascular corrosion casts confirmed this result (Figure 4G). Notably, the distance separating BVs in the diaphysis demonstrated an average separation of 46 ± 3.9 μm (n = 5), which is not significantly different ($P = .1$) from the BV separation in the metaphysis (Figure 4F). Therefore, HSPCs within the diaphysis are also within 3 cell diameters of a BV.

The preferential homing of transplanted HSPCs to the metaphysis is independent of the proportion of extravascular space and BV number and diameter

The spatial distribution of transplanted HSPCs would be influenced by differences in the proportion of extravascular marrow within different regions of BM. To determine whether the proportion of extravascular marrow within the metaphyseal and diaphyseal regions differ, micrographs of the longitudinal femoral sections previously viewed for spatial distribution determinations from 32 recipients were segmented and analyzed. This process was performed in 2 steps, first to segment the bone to form a binary mask and second to segment BVs. This analysis showed that the metaphyses composed 35% ± 1.8% of total extravascular marrow. As described in "Transplanted HSPCs preferentially home to the trabecular-rich metaphysis," 71% ± 1.8% (95% confidence interval, 67.3%-74.0%) of transplanted HSPCs homed to the metaphyses during the first 15 hours after transplantation. This is significantly greater than would be expected on the basis of the proportion of extravascular marrow within this region.

The distribution of HSPCs after transplantation could also be significantly influenced by the number or average width of BVs. Comparison of the overall numbers of BVs per square millimeter (metaphysis: 279 ± 20.4, n = 10; diaphysis: 258 ± 41, n = 5) (Figure 4H) and average BV widths (metaphysis: 27.12 ± 1.6 μm, n = 10; diaphysis: 21.67 ± 1.8 μm, n = 5; Figure 4I) revealed no significant difference between the metaphysis and diaphysis. Based on our collective analysis of bone and BV parameters, there is compelling evidence that HSPCs preferentially home to the metaphysis. In an attempt to understand the mechanism responsible for this, we analyzed cell adhesion molecules (CAMs) involved in HSPC homing.

Downloaded from http://ashpublications.net/blood/article-pdf/118/6/1516/1347016/zh803211001516.pdf by guest on 02 June 2024

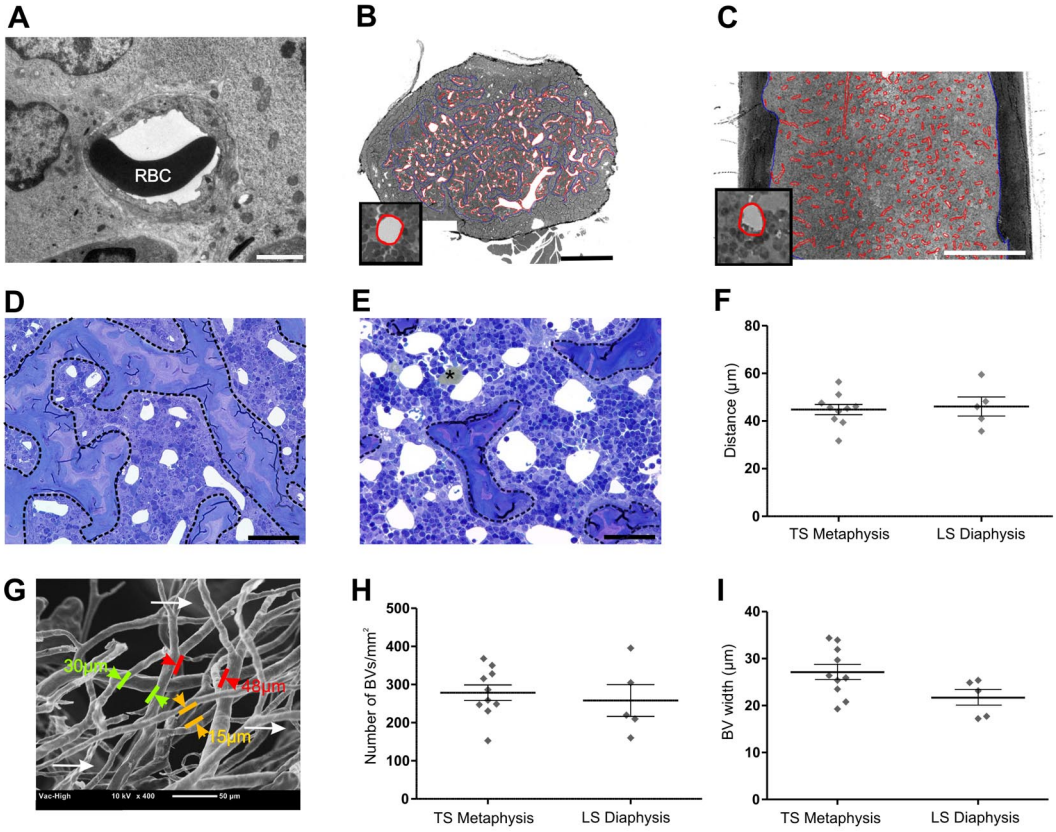

Figure 4. HSPCs within the metaphysis are close to BVs. Homing of HSPCs to the metaphysis is independent of the number and width of BM BV and distance between BVs. (A) Transmission electron micrograph revealing excellent preservation of BVs after perfusion fixation and embedding femurs in resin. RBC indicates red blood cell. Scale bar represents 2 μm. The orientation of BVs within the femur is taken into account for histomorphometric analyses. To obtain cross-sectional profiles of the BVs, femurs are cut transversely through the metaphysis (B) and longitudinally through the diaphysis (C). (B-C) Micrographs represent montages of more than or equal to 48 images captured at high magnification (40× objective, UPlanApo NA 0.85) using the Metamorph "slide scan" function on an Olympus IX81 microscope. Metamorph was used to automatically segment perfusion-cleared individual BVs, which are easily identified at full resolution. Vessels are outlined in red as shown at higher magnification in the insets of panels B and C. Cortical bone and trabeculae are outlined manually in blue. Scale bar represents 0.5 mm. BVs proximal to the growth plate (D) are smaller than those distal from the growth plate (E), where the main central sinus branches into the smaller metaphyseal vessels. Calculation of the distance between individual BVs assumes that most BVs are round and evenly distributed, as exemplified in both panels D and E. BVs are cleared of blood, enabling their clear identification. (E) *Lipid is well preserved because of osmium secondary fixation and cannot be confused with BVs (white areas). The trabecular bone is delineated by a dashed line. Micrographs were captured using a 40× (UPlanApo NA 0.85) objective on an Olympus BX51 microscope fitted with a SPOT RT-SE6 camera. Scale bar represents 50 μm. (B-E) Resin sections (1-μm toluidine blue-stained). (F) Histomorphometric analyses of 1 μm resin sections reveal the distance between BVs within the metaphysis and diaphysis. Each symbol represents individual mice. Data are mean ± SEM. (G) Scanning electron microscopy of vascular casts. Larger-diameter vessels indicative of the early branches of the central sinus are visible below the plane of focus (arrows). The micrograph shown is representative of 5 individual BV casts. (H) Average number of BVs/mm^2 of cellular marrow is comparable between the metaphysis and the diaphysis. (I) The average widths of BVs in the metaphysis and diaphysis are not significantly different. Symbols represent individual mice. Experimental repeats ≥ 3. Data are shown as mean ± SEM.

HA affects the spatial distribution of transplanted HSPCs immediately after transplant

The preferential homing of HSPCs to the metaphysis was observed within 15 minutes after transplantation, suggesting that CAMs on the vasculature are involved in directing HSPCs to the BM trabecular-rich regions. To investigate this, we compared the expression of several CAMs previously identified as being involved in HSPC homing: P-selectin,[26] annexin II,[27] ICAM-1,[28] ICAM-2,[29] and VCAM-1[26,28,30,31] within diaphyseal and metaphyseal BM. All CAMs were ubiquitously expressed throughout the femoral vasculature (supplemental Figure 1), suggesting that their expression on BV endothelium does not account for the preferential distribution of transplanted HSPCs to the metaphysis. In addition to the CAMs listed earlier in this paragraph, the distribution of the chemokine SDF-1, reported to be important in HSC homing,[32-34] was examined. Although SDF-1 was observed on megakaryocytes and a subset of bone lining cells (supplemental Figure 1 inset), it was not observed on the luminal surface of BM sinusoidal endothelium.

We next examined HA and Opn expression to determine whether they might influence the early stages of HPSC homing. Both HA and Opn are highly expressed along the endosteum[19,35-38] and affect the spatial distribution of HSPCs after transplantation.[35,39] More recently, Opn has been demonstrated to exert a strong chemokinetic affect on HSPCs[40] in vitro, and HA expression has been shown on both human and murine BV endothelium.[19,38] Herein, we confirmed strong expression of both molecules at the endosteum with higher levels of expression in the trabecular-rich metaphysis because of increased bone volume (Figure 5A-B). Using mice devoid of either Opn or Has3, the HA synthase predominantly responsible for the expression of HA in the endosteal region and critical for HSC lodgement,[41] we examined the spatial and temporal dynamics of transplanted wild-type (WT) HSPCs 15 minutes and 45 minutes after transplantation in these mice.

Analysis of homing efficiency, including correcting for HSPC within vessels, revealed no statistical differences in the proportion of HSPCs homed to BM in Opn$^{-/-}$ and Has3$^{-/-}$ recipients compared with WT at either 15 minutes or 45 minutes after

Downloaded from http://ashpublications.net/blood/article-pdf/118/6/1516/1347016/zh803211001516.pdf by guest on 02 June 2024

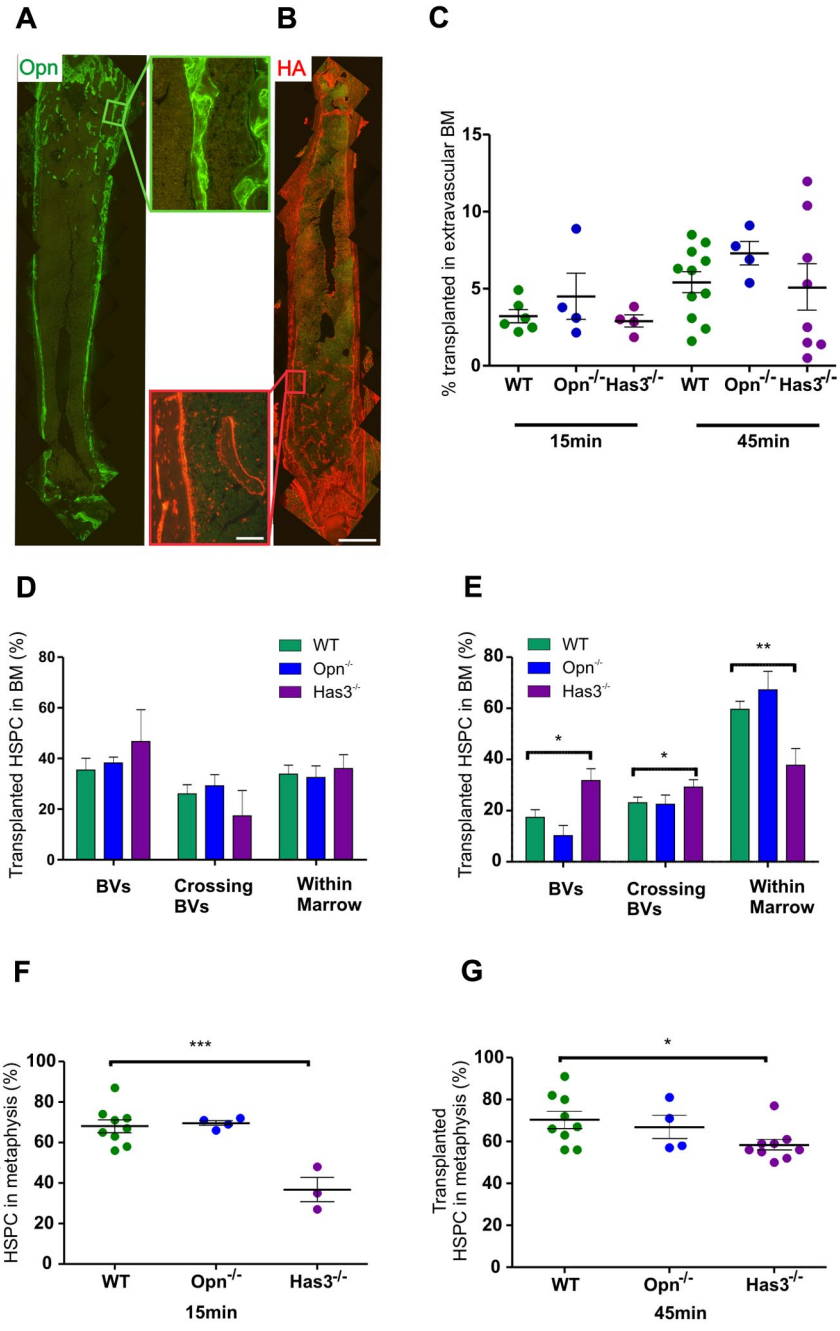

Figure 5. Opn and HA are highly expressed in the metaphysis and endosteal regions. Has3-synthesized HA significantly affects the ability of HSPC to transendothelially migrate into the metaphysis region at very early time points after transplantation. (A) Immunohistochemical staining of longitudinal femoral sections reveals strong expression of Opn around trabeculae in the metaphysis as evidenced at higher magnification (boxed region to the right of the image). (B) HA binding protein reveals strong expression of HA around trabeculae in the metaphysis as evidenced at higher magnification (boxed region to the left of the image). Scale bar represents 1 mm (low magnification images) and 100 μm (higher magnification images). Micrographs captured using a 10× (UPLSApo NA 0.4) objective on an Olympus BX51 microscope fitted with a SPOT RT-SE6 camera. Montages constructed with Photoshop CS2. (C) Homing of transplanted HSPC to the extravascular BM in recipients devoid of either Has3-synthesized HA or Opn. Data are corrected for the proportion of HSPC in BVs. (D) The distribution of HSPCs within the femur of recipients devoid of Has3-synthesized HA reveals an increased percentage in the BVs of Has3$^{-/-}$ recipients compared with WT at 15 minutes after transplantation. (E) At 45 minutes, there is a statistically significant increase in the percentage of HSPCs within the BVs of Has3$^{-/-}$ recipients, with a concomitant decrease in HSPCs within the cellular marrow. There is also a significantly higher percentage of HSPC crossing the BVs in Has3$^{-/-}$ recipients: WT 15 minutes, n = 7; Opn$^{-/-}$ 15 minutes, n = 4; Has3$^{-/-}$ 15 minutes, n = 3. WT 45 minutes, n = 8; Opn$^{-/-}$ 45 minutes, n = 4; Has3$^{-/-}$ 45 minutes, n = 9. Experimental repeats more than or equal to 3. *P = .01 (in BV). *P = .03 (crossing BVs). **P = .005 (in extravascular BM). (F) Homing of HSPCs in Has3$^{-/-}$ recipients exhibited an aberrant distribution with significantly less HSPC homing to the metaphysis. ***P < .001. (G) The spatial distribution defect was still evident after 45 minutes. *P = .02. (F-G) Symbols represent individual recipients. Experimental repeats ≥ 3. Data are mean ± SEM. See also supplemental Figures 1-3.

transplantation (Figure 5C). Examination of the precise location of HSPCs within the marrow did not reveal statistically different proportions of HSPC residing in vessels, crossing the sinusoidal endothelium, or in extravascular BM after transplantations into either Opn$^{-/-}$ and Has3$^{-/-}$ recipients at 15 minutes after transplant. There was, however, a trend suggesting increasing proportions of HSPC remaining in vessels of Has3$^{-/-}$ compared with WT recipients (47% ± 12% Has3$^{-/-}$ recipients vs 35% ± 5% WT recipients; Figure 5D). By 45 minutes after transplantation, this trend was statistically different (32% ± 4% vs 17% ± 3%, respectively, P = .01; Figure 5E), and there was a concomitant decrease in the proportion of HSPCs within cellular marrow (36% ± 6% Has3$^{-/-}$ recipients vs 60% ± 3% WT recipients, P = .005). There were also more HSPCs undergoing transendothelial migration in Has3$^{-/-}$ recipients (31% ± 3% Has3$^{-/-}$ recipients vs 23% ± 2% WT recipients, P = .03). Together, these data suggest that HSPCs take longer to physically transendothelially migrate into BM in the absence of Has3-synthesized HA.

In addition, we observed an aberrant distribution of transplanted HSPCs in Has3$^{-/-}$ recipients compared with WT 15 minutes after transplantation, with significantly fewer HSPCs located within the metaphysis (37% ± 6% vs 68% ± 3%, respectively, P = .0006; Figure 5F). This significant difference was still evident 45 minutes after transplantation (58% ± 3% Has3$^{-/-}$ recipients vs 70% ± 4% WT recipients, P = .02; Figure 5G), suggesting that HA in the metaphysis plays an important role in HSPC homing. To exclude the possibility that these differences were the consequence of differences in BV parameters, BV width, total BV numbers, and the distance separating BVs within the metaphysis of Has3$^{-/-}$ mice were examined. No significant differences in any of these parameters

Downloaded from http://ashpublications.net/blood/article-pdf/118/6/1516/1347016/zh803211001516.pdf by guest on 02 June 2024

were detected (supplemental Figure 2). In addition, the expression of CAMs on the sinusoidal endothelium of Has3$^{-/-}$ marrow was examined. No differences in the expression of ICAM-1, ICAM-2, annexin II, P-selectin, or VCAM-1 were detected between WT and Has3$^{-/-}$ marrow (supplemental Figure 3). Collectively, these data demonstrate that Has3-synthesized HA is important during the early stages of homing and specifically transendothelial migration of HSPCs to the metaphysis.

Discussion

In this study, we show that endosteal and vascular HSC niches are not mutually exclusive in the metaphysis. We analyzed the physical relationships between bone, vasculature, and transplanted HSPCs at the individual cell level. Unlike intravital imaging methodologies, our experimental approach, which combines micro-CT, histomorphometry, and spatial distribution assays, avoids prolonged anesthesia, inflammation, and damage to bone and/or marrow, all of which have unknown and variable effects on HSPC homing. In addition, whereas intravital imaging is limited in penetration depth and area, our approach permits the examination of transplanted HSPCs at the individual cell level throughout the entire length of the femur. We reveal that HSPCs preferentially and consistently transendothelially migrate in the metaphysis, between 15 minutes and 15 hours after transplantation and are directed to this region, in part, by Has3-synthesized HA.

In the current study, we used HSPCs defined by the LSK phenotype for spatial distribution and homing assays because of the number of cells required to be able to accurately track them after transplantation. The use of cells with this phenotype for these assays has been previously validated by us, using a functional enrichment strategy, based on the ability of cells with long-term multilineage reconstitution to home to the endosteal region of nonablated recipients at very short time points after transplantation.[20] The use of this functional selection increased the frequency of long-term multilineage HSCs in the endosteal LSK population from 1:259 to 1:12. Together, these data demonstrate that analysis of cells in the endosteal region at short time points after a transplantation of cells with the LSK phenotype will indeed be analyzing a much higher frequency of cells capable of long-term multilineage reconstitution than that initially transplanted, and one not dissimilar to the LSKCD150^{+}CD48^{-} phenotype.

The preferential homing of transplanted HSPCs to the trabecular-rich metaphysis in nonablated recipients confirms and extends the recent findings of Jiang et al[42] who reported approximately 83% HSPCs (Lin^{-}Sca^{+}) homed to trabecular-rich regions of BM 20 hours after transplantation. Preferential homing of HSPCs to the metaphysis was shown herein to be an active process and independent of differing proportions of marrow between the metaphysis and diaphysis or to differences in the average BV width, number of BVs/mm^2, or distance separating BVs within the metaphysis and diaphysis. In contrast to our findings and that of Jiang et al,[42] another study[10] recently reported that transplanted HSPCs did not home preferentially to trabecular-rich regions in nonablated mice. The reasons for this conflicting data are unclear but could be because of the significant difference in the number of HSPCs examined between the studies and/or their use of a more highly purified population of HSPCs. Xie et al[10] analyzed a total of 26 HSPCs in an undefined number of recipients 5 to 8 hours after transplantation, whereas we analyzed between 131 HSPCs (5-hour time point) and 827 HSPCs (15-hour time point) with a total of 2426 HSPCs from 30 individual mice over a 15-hour time period. In support of our observations, which were derived from transplants of HSPCs defined by an LSK phenotype, a number of other studies using populations of HSPCs variably enriched for HSCs have also demonstrated a nonrandom distribution of transplanted HSPCs in nonablated recipients to the endosteal regions of bone.[3,7-9,18,20,33,39,43-45]

To characterize the microanatomic location of HSPCs within the metaphysis, we analyzed the relationships between bone, BVs, and HSPC. Micro-CT permitted noninvasive imaging of the metaphyseal trabeculae in 3 dimensions and demonstrated that HSPCs in the metaphysis exist in an endosteal niche, as previously defined by us and others as within 12 cell diameters from the bone.[3,18,22-24] Histomorphometric analyses of BVs in resin sections showed that all HSPCs within the metaphysis are < 3 cell diameters from a BV. Taken together, these data demonstrate that HSPCs within the metaphysis exist in an endosteal niche where they lie in close proximity to BVs. In this region of the BM, BVs do not form a separate niche but are an integral part of the endosteal niche. Although the concept of a combined endosteal and vascular niche has been suggested by several other studies,[9,10,23,46-48] we definitively demonstrate this, using a nondestructive method and through analysis of HSPC homing throughout the full length of the femur. Within the endosteal niche, it is also possible that highly localized cell-cell or cell-matrix contacts exist and that these may play a key role in HSPC regulation. However, the aim of this manuscript is not to further define and characterize the final resting site of transplanted HSPCs.

The spatial distribution of transplanted HSPCs at the single-cell level identifies HSPCs within BVs, crossing the sinusoidal endothelium, or within the BM extravascular space and permits correction of homing efficiency calculations by standard flow cytometric analysis. Herein, we reveal the actual percentage of transplanted HSPC within BM extravascular space during the first 15 hours after transplantation in a nonablated setting, demonstrating that the recruitment of these cells to the BM after transplantation is a gradual process. These data are consistent with a recent study detailing the homing kinetics of HSPCs in an ablated setting.[11] In accord with previous intravital studies of HSPCs homing within the trabecular calverium,[9] homing of transplanted HSPCs to long bones under physiologic conditions is rapid with evidence of HSPCs within BM 15 minutes after transplantation.

As transplanted HSPCs home preferentially to the metaphysis within 15 minutes after transplantation, it suggests that the vascular endothelium in this region might express a unique repertoire of CAMs. The ubiquitous expression of P-selectin, annexin II, ICAM-1, ICAM-2, and VCAM-1 on the sinusoidal endothelium throughout the full length of the femur suggests the involvement of additional molecules in directing the homing of transplanted HSPCs to the metaphysis. However, it should be noted that functional differences in any of these endothelial expressed CAMs in different BM regions may be playing an as yet unrecognized role in HSPC homing. Because of the well-described role of the chemokine, SDF-1, in HSC migration, we analyzed its expression on sinusoidal endothelium within the different BM regions. Similar to previous publications,[15,49] we did not detect this molecule on the luminal surface of the murine BV endothelium, despite the use of 4 different antibodies to SDF-1 and using both in situ and in vivo labeling methods. The lack of SDF-1 expression on murine BV endothelium is somewhat unexpected, with previous reports suggesting that it is expressed on the BV endothelium of SCID[7,33] and NOD/SCID mice.[34]

Downloaded from http://ashpublications.net/blood/article-pdf/118/6/1516/1347016/zh803211001516.pdf by guest on 02 June 2024

Two molecules, the glycoprotein Opn and the glycosaminoglycan HA, were selected as candidates capable of directing transplanted HSPCs to the metaphysis based on their previously reported high expression in the metaphysis[19,39,40] as well as their influence on the spatial distribution of HSPCs 15 hours after transplantation.[35,39] In addition, Opn has recently been revealed as a powerful HSPC chemoattractant in vitro.[40] Extending these studies, the work herein reveals that Opn does not have a role in directing transplanted HSPCs to the metaphysis at time points immediately after transplantation and supports the earlier findings that more HSPCs reside in the central BM regions of $Opn^{-/-}$ mice immediately after transplantation.[39]

HA is expressed on both human[38] and murine[19] vascular endothelium and, as shown herein, is highly expressed around trabecular bone within the metaphysis. Blocking the major receptor for HA, CD44, on human HSPC ($CD34^+$) with monoclonal antibodies or soluble HA, decreased HSPC homing into irradiated NOD/SCID mice by 70%-80% 16 hours after transplantation. In addition, immediate pretreatment of recipients with hyaluronidase also decreased homing by 40%.[38] Avigdor et al[38] revealed HA as a major player in the homing of human HSPC in NOD/SCID recipients but does not reveal the level at which this occurs, transendothelial migration, transmarrow migration, or retention within the endosteal niche. Nor is it known which HA synthase is involved in this process. Our spatial distribution analyses of WT HSPCs transplanted into $Has3^{-/-}$ recipients 15 minutes after transplantation revealed a statistically significant redistribution with 30% less HSPCs in the metaphysis compared with WT recipients. This aberrant distribution was still apparent 45 minutes after transplantation. Furthermore, a significantly increased proportion of HSPCs within blood vessels of $Has3^{-/-}$ recipients and a concomitant decrease in the proportion of HSPC in extravascular BM of $Has3^{-/-}$ compared with WT recipients at 45 minutes after transplantation strongly suggest a key role for this glycosaminoglycan in HSPC transendothelial migration. Although it is possible that other HA synthases are compensating for the absence of Has3 in some way, the significant changes in homing to BM observed in $Has3^{-/-}$ compared with control mice is occurring in the presence of HA synthesized by both Has1 and Has2 synthases. Therefore, if such compensation is occurring, it is not sufficient to modulate these observed changes in homing.

Our data demonstrate the power of analyzing HSPC homing at the single-cell level throughout the full length of long bones to reveal subtle differences between WT and knockout recipients. Taken together, we have identified an important role for Has3-synthesized HA in directing homing of transplanted HSPCs to the metaphysis during very early stages of homing, putatively through interactions between HSPCs and HA expressed on BV. Future investigations are aimed at identifying other molecules involved in directing HSPCs to the metaphysis.

In conclusion, we show that HSPCs preferentially home to the trabecular-rich metaphysis in the femur of nonablated recipients with this distribution evident within 15 minutes after transplantation. Significantly, within the metaphysis, all HSPCs exist in an endosteal niche in close proximity to blood vessels, which do not form a separate niche. The use of novel approaches has allowed the assessment of HSPC homing and lodgement at the single-cell level, revealing a key role for Has3-synthesized HA in HPSC transendothelial migration during early stages of homing.

Acknowledgments

The authors thank Brenda Williams, Gemma Olsen, and Dani Cordozo (Commonwealth Scientific and Industrial Research Organization), Flow Cytometry staff of the Australian Stem Cell Center, and Histology staff from the Peter MacCallum Cancer Center Microscopy Core for excellent technical help and support, Andrew Ellis (Austin Hospital) for critically reading the manuscript, and Alan Herschtal (Statistics Department, Peter MacCallum Cancer) for assistance with statistical analysis.

This work was supported by the Australian Stem Cell Centre (S.K.N. and D.H.).

Authorship

Contribution: S.L.E. designed and performed experiments, analyzed the data, and wrote the manuscript; J.G., J.B., and S.K.N. performed experiments; A.J. and T.C. contributed vital analytical tools; and S.K.N., I.B., and D.H. designed experiments and critically reviewed the manuscript.

Conflict-of-interest disclosure: The authors declare no competing financial interests.

Correspondence: Susan K. Nilsson, Commonwealth Scientific and Industrial Research Organization, Ian Wark Laboratory, Bag 10, Clayton South MDC, Victoria 3169 Australia; e-mail susie.nilsson@csiro.au.

References

1. Schofield R. The relationship between the spleen colony-forming cell and the haemopoietic stem cell. *Blood Cells.* 1978;4(1):7-25.
2. Calvi LM, Adams GB, Weibrecht KW, et al. Osteoblastic cells regulate the haematopoietic stem cell niche. *Nature.* 2003;425(6960):841-846.
3. Nilsson SK, Dooner MS, Tiarks CY, Weier H-UG, Quesenberry PJ. Potential and distribution of transplanted hematopoietic stem cells in a nonablated mouse model. *Blood.* 1997;89(11):4013-4020.
4. Visnjic D, Kalajzic Z, Rowe DW, Katavic V, Lorenzo J, Aguila HL. Hematopoiesis is severely altered in mice with an induced osteoblast deficiency. *Blood.* 2004;103(9):3258-3264.
5. Zhang J, Niu C, Ye L, et al. Identification of the haematopoietic stem cell niche and control of the niche size. *Nature.* 2003;425(6960):836-841.
6. Kiel MJ, Yilmaz OH, Iwashita T, Yilmaz OH, Terhorst C, Morrison SJ. SLAM family receptors distinguish hematopoietic stem and progenitor cells and reveal endothelial niches for stem cells. *Cell.* 2005;121(7):1109-1121.
7. Sipkins DA, Wei X, Wu JW, et al. In vivo imaging of specialized bone marrow endothelial microdomains for tumour engraftment. *Nature.* 2005;435(7044):969-973.
8. Kohler A, Schmithorst V, Filippi M-D, et al. Altered cellular dynamics and endosteal location of aged early hematopoietic progenitor cells revealed by time-lapse intravital imaging in long bones. *Blood.* 2009;114(2):290-298.
9. Lo Celso C, Fleming HE, Wu JW, et al. Live-animal tracking of individual haematopoietic stem/progenitor cells in their niche. *Nature.* 2009;457(7225):92-96.
10. Xie Y, Yin T, Wiegraebe W, et al. Detection of functional haematopoietic stem cell niche using real-time imaging. *Nature.* 2009;457(7225):97-101.
11. Lewandowski D, Barroca V, Duconge F, et al. In vivo cellular imaging pinpoints the role of reactive oxygen species in the early steps of adult hematopoietic reconstitution. *Blood.* 2010;115(3):443-452.
12. Suzuki N, Ohneda O, Minegishi N, et al. Combinatorial Gata2 and Sca1 expression defines hematopoietic stem cells in the bone marrow niche. *Proc Natl Acad Sci U S A.* 2006;103(7):2202-2207.
13. Brookes M. *The Blood Supply of Bone.* London, United Kingdom: Butterworths; 1971.
14. Kollet O, Shivtiel S, Chen Y-Q, et al. HGF, SDF-1, and MMP-9 are involved in stress-induced human $CD34^+$ stem cell recruitment to the liver. *J Clin Invest.* 2003;112(2):160-169.
15. Ponomaryov T, Peled A, Petit I, et al. Induction of the chemokine stromal-derived factor-1 following

Downloaded from http://ashpublications.net/blood/article-pdf/118/6/1516/1347016/zh803211001516.pdf by guest on 02 June 2024

DNA damage improves human stem cell function. *J Clin Invest.* 2000;106(11):1331-1339.

16. Mazo IB, Quackenbush EJ, Lowe JB, von Andrian UH. Total body irradiation causes profound changes in endothelial traffic molecules for hematopoietic progenitor cell recruitment to bone marrow. *Blood.* 2002;99(11):4182-4191.
17. Mazo IB, Gutierrez-Ramos JC, Frenette PS, Hynes RO, Wagner DD, von Andrian UH. Hematopoietic progenitor cell rolling in bone marrow microvessels: parallel contributions by endothelial selectins and vascular cell adhesion molecule 1. *J Exp Med.* 1998;188(3):465-474.
18. Nilsson SK, Johnston HM, Coverdale JA. Spatial localization of transplanted hemopoietic stem cells: inferences for the localization of stem cell niches. *Blood.* 2001;97(8):2293-2299.
19. Ellis SL, Williams B, Asquith S, Bertoncello I, Nilsson SK. An innovative triple immunogold labeling method to investigate the hemopoietic stem cell niche *in situ. Microsc Microanal.* 2009; 15(5):403-414.
20. Grassinger J, Haylock DN, Williams B, Olsen GH, Nilsson SK. Phenotypically identical hemopoietic stem cells isolated from different regions of bone marrow have different biological potential. *Blood.* 2010;116:3185-3196.
21. Smith LH, Clayton ML. Distribution of injected ^{59}Fe in mice. *Exp Hematol.* 1970;20:82-86.
22. Méndez-Ferrer S, Michurina TV, Ferraro F, et al. Mesenchymal and haematopoietic stem cells form a unique bone marrow niche. *Nature.* 2010; 466(7308):829-834.
23. Bourke VA, Watchman CJ, Reith JD, Jorgensen ML, Dieudonne A, Bolch WE. Spatial gradients of blood vessels and hematopoietic stem and progenitor cells within the marrow cavities of the human skeleton. *Blood.* 2009;114(19):4077-4080.
24. Jung Y, Shiozawa Y, Wang J, et al. Annexin-2 is a regulator of stromal cell-derived factor-1/CXCL12 function in the hematopoietic stem cell endosteal niche. *Exp Hematol.* 2011;39(2):151-166.
25. De Bruyn PPH, Breen PC, Thomas TB. The microcirculation of the bone marrow. *Anat Rec.* 1970;168(1):55-68.
26. Frenette PS, Subbarao S, Mazo IB, von Andrian UH, Wagner DD. Endothelial selectins and vascular cell adhesion molecule-1 promote hematopoietic progenitor homing to bone marrow. *Proc Natl Acad Sci U S A.* 1998;95(24):14423-14428.
27. Jung Y, Wang J, Song J, et al. Annexin II expressed by osteoblasts and endothelial cells regulates stem cell adhesion, homing and engraftment following transplantation. *Blood.* 2007; 110(1):82-90.
28. Peled A, Grabovsky V, Habler L, et al. The chemokine SDF-1 stimulates integrin-mediated arrest of CD34$^+$ cells on vascular endothelium under shear flow. *J Clin Invest.* 1999;104(9): 1199-1211.
29. Chilton PM, Rezzoug F, Ratajczak MZ, et al. Hematopoietic stem cells from NOD mice exhibit autonomous behavior and a competitive advantage in allogeneic recipients. *Blood.* 2005;105(5): 2189-2197.
30. Imai K, Kobayashi M, Wang J, et al. Selective transendothelial migration of hematopoietic progenitor cells: a role in homing of progenitor cells. *Blood.* 1999;93(1):149-156.
31. Papayannopoulou T, Craddock C, Nakamoto B, Priestley GV, Wolf NS. The VLA4 / VCAM-1 adhesion pathway defines contrasting mechanisms of lodgement of transplanted murine hemopoietic progenitors between bone marrow and spleen. *Proc Natl Acad Sci U S A.* 1995;92:9647-9651.
32. Kollet O, Spiegel A, Peled A, et al. Rapid and efficient homing of human CD34$^+$CD38$^{-/low}$CXCR4$^+$ stem and progenitor cells to the bone marrow and spleen of NOD/SCID and NOD/SCID/B2m^{null} mice. *Blood.* 2001;97(10):3283-3291.
33. Colmone A, Amorim M, Pontier AL, Wang S, Jablonski E, Sipkins DA. Leukemic cells create bone marrow niches that disrupt the behavior of normal hematopoietic progenitor cells. *Science.* 2008;322(5909):1861-1865.
34. Dar A, Goichberg P, Shinder V, et al. Chemokine receptor CXCR4-dependent internalization and resecretion of functional chemokine SDF-1 by bone marrow endothelial and stromal cells. *Nat Immunol.* 2005;6(10):1038-1046.
35. Nilsson SK, Haylock DN, Johnston HM, Occhiodoro T, Brown TJ, Simmons PJ. Hyaluronan is synthesized by primitive hemopoietic cells, participates in their lodgment at the endosteum following transplantation, and is involved in the regulation of their proliferation and differentiation in vitro. *Blood.* 2003;101(3):856-862.
36. Chen J, Singh K, Mukherjee BB, Sodek J. Developmental expression of osteopontin (OPN) mRNA in rat tissues: evidence for a role for OPN in bone formation and resorption. *Matrix.* 1993; 13(2):113-123.
37. Stier S, Ko Y, Forkert R, et al. Osteopontin is a hematopoietic stem cell niche component that negatively regulates stem cell pool size. *J Exp Med.* 2005;201(11):1781-1791.
38. Avigdor A, Goichberg P, Shivtiel S, et al. CD44 and hyaluronic acid cooperate with SDF-1 in the trafficking of human CD34$^+$ stem/progenitor cells to bone marrow. *Blood.* 2004;103(8):2981-2989.
39. Nilsson SK, Johnston HM, Whitty GA, et al. Osteopontin, a key component of the hematopoietic stem cell niche and regulator of primitive hematopoietic progenitor cells. *Blood.* 2005;106(4):1232-1239.
40. Grassinger J, Haylock DN, Storan MJ, et al. Thrombin-cleaved osteopontin regulates hemopoietic stem and progenitor cell functions through interactions with alpha9beta1 and alpha4beta1 integrins. *Blood.* 2009;114(1):49-59.
41. Haylock DN, Nilsson SK. The role of hyaluronic acid in hemopoietic stem cell biology. *Regen Med.* 2006;1(4):437-445.
42. Jiang Y, Bonig H, Ulyanova T, Chang K, Papayannopoulou T. On the adaptation of endosteal stem cell niche function in response to stress. *Blood.* 2009;114(18):3773-3782.
43. Haylock DN, Williams B, Johnston HM, et al. Hemopoietic stem cells with higher hemopoietic potential reside at the bone marrow endosteum. *Stem Cells.* 2007;25(4):1062-1069.
44. Yoshimoto M, Shinohara T, Heike T, Shiota M, Kanatsu-Shinohara M, Nakahata T. Direct visualization of transplanted hematopoietic cell reconstitution in intact mouse organs indicates the presence of a niche. *Exp Hematol.* 2003;31(8): 733-740.
45. Zhong JF, Zhan Y, Anderson WF, Zhao Y. Murine hematopoietic stem cell distribution and proliferation in ablated and nonablated bone marrow transplantation. *Blood.* 2002;100(10):3521-3526.
46. Hooper AT, Butler JM, Nolan DJ, et al. Engraftment and reconstitution of hematopoiesis is dependent on VEGFR2-mediated regeneration of sinusoidal endothelial cells. *Cell Stem Cell.* 2009; 4(3):263-274.
47. Watchman CJ, Bourke VA, Lyon JR, et al. Spatial distribution of blood vessels and CD34$^+$ hematopoietic stem and progenitor cells within the marrow cavities of human cancellous bone. *J Nucl Med.* 2007;48(4):645-654.
48. Yahata T, Muguruma Y, Yumino S, et al. Quiescent human hematopoietic stem cells in the bone marrow niches organize the hierarchical structure of hematopoiesis. *Stem Cells.* 2008;26:3228-3236.
49. Sugiyama T, Kohara H, Noda M, Nagasawa T. Maintenance of the hematopoietic stem cell pool by CXCL12-CXCR4 chemokine signaling in bone marrow stromal cell niches. *Immunity.* 2006; 25(6):977-988.

Downloaded from http://ashpublications.net/blood/article-pdf/118/6/1516/1347016/zh803211001516.pdf by guest on 02 June 2024